MicroRNA-126-3P targets PIK3R2 to ameliorate autophagy and apoptosis of cortex in hypoxia–reoxygenation treated neonatal rats

Jingjing Ge, Xiaoling Jiao, Hui Li*

Pediatric Internal Medicine, Yantai Yuhuangding Hospital, Yantai 264000, Shandong, China

ARTICLE INFO	ABSTRACT
	Here, we explored a possible mechanism of microRNA-126-3p (miR-126-3p) on neonatal rats with hypoxia-reoxygenation injury (HI). After administering HI to newborn Sprague-Dawley rats, the expression of miR-126-3p in the brain injury was assessed by RT-PCR. A miR-126-3p mimic and inhibitor were treated in the HI neonatal rats. The water maze test, TTC, HE, Nissl and TUNEL staining were separately implemented to test the effects of miR-126-3p on the HI-treated neonatal rats. At the same time, the phosphoinositide-3-kinase regulatory subunit 2 (PIK3R2) expression in the damaged cortex region was analyzed. *In vitro*, cortical neurons were cultured and treated with oxygen and glucose deprivation (OGD), then transfected miR-126-3p mimic, PIK3R2 overexpression lentivirus vector or silence of PIK3R2. The cell viability was observed by CCK-8. The autophagy of neurons was detected by acridine orange staining. In contrast to the sham-operated rats, the miR-126-3p expression significantly decreased, but PIK3R2 expression markedly rose in the cortex of HI rats. Injection of miR-126-3p mimic raised the learning and memory abilities through down-regulating the cerebral ischemic area, improving pathological damage of the cortex, reducing the neurons apoptosis of the cortex and down-regulating the autophagy-related and apoptosis-related proteins. Overexpression of PIK3R2, a miR-126-3p target, may reduce cell viability and boost autophagy and apoptosis. Silence of PIK3R2 promoted cell viability and inhibited cell apoptosis and autophagy. The consequences of miR-126-3p were comparable to those of PIK3R2 silencing. A new therapeutic target for HI injury in newborn rats is provided by the overexpression of miR-126-3p, which inhibits autophagy and death of cortical neurons by targeting PIK3R2 in HI-treated neonatal rats.

Introduction

One of the more serious conditions affecting the central nervous system in the perinatal era is hypoxic-ischemic brain damage, which is brought on by suffocation or hypoxia, which can cause cerebral palsy, epilepsy and intellectual and hearing impairment or even death if left untreated (1). The brain, particularly the hippocampus, is sensitive to low concentrations of oxygen, which is important for learning and memory (2). In hypoxia-reoxygenation injury (HI), short- or long-term damage to the developing brain may impair these functions. Hippocampal pyramidal neurons are the most vulnerable neuronal cells in HI injury-induced apoptosis, and HI injury to hippocampal neuronal cells may lead to severe neurological deficits due to the important influence of hippocampal structure on cognitive function. This brings a heavy burden to the families of these patients and society. Recent studies have focused on neonatal HI encephalopathy, hoping to obtain more basic and clinical research on the pathogenesis and treatment of neonatal HI encephalopathy, so as to reduce the mortality rate and the chance of neurological sequelae in these children (3).

The pathogenesis of HI brain injury is complex, involving several mechanisms. The occurrence, progression, and regulatory mechanism of HI brain injury have been investigated in various studies. Studies have shown that when ischemia and hypoxia occur in brain tissue, they damage the oxidative defense system of brain tissue and break the balance between oxygen radical production and oxygen scavenging, allowing the body to build up a lot of reactive oxygen species will cause an oxidative stress reaction (4-6). Large amounts of oxygen free radicals, which attack mitochondria, increase mitochondrial permeability and release mitochondrial cytochrome c and apoptosis-inducing factors, leading to neurodegeneration and apoptosis, as well as memory impairment (1). At present, numerous therapies have been utilized in an attempt to resolve brain injury caused by HI. Researches on additional treatment options, such as erythropoietin (7), glutamate receptor antagonist (8), and stem cell transplantation (9) are currently ongoing.

MicroRNA (miRNA) regulates transcription factors by inducing the degradation of miRNA to regulate gene expression. In addition, miRNAs can act as independent transcripts to directly inhibit or increase the translation of target genes, and play a post-transcriptional regulatory role (10) mainly in cell differentiation, metabolism, apoptosis, neuronal development, and other biological processes (11). Ouyang and colleagues demonstrated that the upregulated expression of miR-181 in ischemic focal points promoted cell death in mice with cerebral ischemia (12). Other studies have found that distress hypoxic injury caused a clear decrease in the miR-23b expression

of fetuses, thereby inhibiting the apoptotic peptidase activating factor 1 (APAF1) expression (13). MiR-27a in the course of traumatic brain injury, which played a neuroprotective role by inhibiting forkhead box O3 (FOXO3)-mediated autophagy (14). MiR-126 is an important potential target and regulatory site of ischemia-related angiogenesis and repair signals and also plays significant roles in cell growth, proliferation, and immune regulation (15).

Our study used a newborn Sprague-Dawley rat model of HI and oxygen and glucose deprivation (OGD) to examine the effects of miR-126-3p on cortical neurons and elucidate the associated pathways.

Materials and Methods

Animals

Newborn Sprague–Dawley rats of either sex (age: 7 days; weight: 13-19 g) (Beijing Vital River Laboratory Animal Technology Co., Ltd. SCXK (Jing) 20160006). Conditions included standard nutrition (23±2°C, 55±5% relative humidity) with a 12-h light-dark cycle. All animal care refers to the guidelines of the National Institutes of Health (NIH publication no. 85-23, revised 1996). These animal experiments were agreed upon by the Animal Care and Use Committee of the Affiliated Yantai Yuhuangding Hospital of Qingdao University.

HI Model

As previous description (6), the left common carotid artery of neonatal rats was permanently ligated while they were under sevoflurane anesthesia. The operation time was dominated within 5 minutes, and neonatal rats went back to their mothers for 2 hours after waking. Then, the pups underwent perfusion with 8% O_2/92% N_2 for 120 min at 37°C. There was no occurrence of death during this process. Subsequently, the rats were fed as usual. Brain tissues were collected 24 hours or 34 days post-HI.

Animals Groups

On the basis of the random number table, 168 neonatal rats were taken into 6 groups (28 in each group, 14 males and 14 females), including sham group, HI group, miR-126-3p mimic (MiR-126-3p) group, mimic negative control (MiR-126-3p NC) group, inhibitor group, and inhibitor negative control (Inhibitor NC) group.

Neonatal rats in the sham group had the same procedure without ligation. In the miR-126-3p group, neonatal rats were treated with 10 μM miR-126-3p mimic before HI operation 48 hours, at 12-hour intervals, a total of 4 times (16). In the miR-126-3p NC group, neonatal rats were treated with 10 μM mimic negative control before HI operation 48 hours, at 12-hour intervals, a total of 4 times (16). In the inhibitor group, neonatal rats were administrated with 10 μM miR-126-3p inhibitor before HI operation 48 hours, at 12-hour intervals, a total of 4 times (16). In the inhibitor NC group, neonatal rats were administrated with 10 μM inhibitor negative control before HI operation 48 hours, at 12-hour intervals, a total of 4 times (16). The neonatal rats were anesthetized with 3% isoflurane (16). For each dose, the neonatal rats were injected at 8:00 a.m. and 8:00 p.m. through intraventricular stereotactic injection (2 mm posterior, 1.5 mm lateral, 3 mm below the skull surface) before establishing the HI model (17). After the 4th dose, the HI model was established at 8:00 a.m. on the second day.

Samples collection

Twenty-four hours post-HI, neonatal rats (12/each group) were anesthetized by sevoflurane and sacrificed. The brain tissues were collected at 4°C. Some tissues (n=6, each group) were stored at −80°C for RT-PCR and western blot, while others were used for TTC staining.

2,3,5-TTC Staining

After 10 minutes of being frozen at -20°C, the entire brain tissue was cut into 5 slices. Slices were incubated with a 2% TTC solution for 30 min at 25°C. The images of slices were pictured and analyzed by ImagePro Plus software. The infarct volume (%) = cerebral infarction volume / total cerebral volume × 100%.

RT-PCR

After 24 hours post-HI, cortex tissues of the left brain were collected from the brains. Tissues were homogenized and centrifuged at 4°C (1000 ×g, 20 min) for further detection. A Trizol Kit (R0016, Beyotime, Shanghai, China) was used to extract total RNA, and a BeyoFast™ probe one-step qRT-PCR kit (D7277M, Beyotime, Shanghai, China) was used to transcribe cDNA. According to the $2^{-\Delta\Delta Ct}$ method, the results of target mRNAs were calculated. The sequences of primers of this experiment are shown in Table 1.

Western Blotting

The cortex tissue of the left brain after 24 hours post-HI or cells treated in each group were centrifuged (1000 ×g, 15 min) to obtain the supernatants. After analyzing the concentration of protein, the protein sample was electrophoresed on SDS-PAGE and then transferred to the membrane. After blocking, add PIK3R2 (1:500, orb76194, Biorbyt, Cambridge, UK), LC3B (1:1,000; 2775S, Cell Signaling Technology, Danvers, MA, USA), Beclin1 (1:1,000; 3738s, Cell Signaling Technology, Danvers, MA, USA), p62 (1:500, orb89844), Cleaved-capase-3 (1:500, orb106556), Bax (1:500, orb224426), Bcl-2 (1:500, orb228150), β-actin (1:2000, orb178392) for incubation. p62, Cleaved-capase-3, Bax, Bcl-2 and β-actin are all from Biorbyt. Finally, it was incubated with goat anti-rabbit IgG antibody (1:1,000; ABIN101988) for 60 minutes. For 3-5 minutes, the membranes were seen using an ECL luminous substrate. Using ImagePro Plus, proteins were scanned, measured, and normalized to β-actin.

Morris Water Maze

29 days after HI, the positioning navigation experiment and spinal exploration experiment were carried out. The water temperature was 25 ± 1°C, and the light source and reference objects were consistent during the experiment. Positioning navigation experiment: A fixed water entry point was demarcated in the pool. The moment the rats realized they were on a platform was timed after they were thrown into the pool with their heads facing the wall. If the period was longer than 90 seconds, the rats were instructed to find the platform and to remain there for 20 seconds. Each rat was recorded for 5 consecutive days, 4 times/day. Spinal exploration experiment: Rats were dropped into the water from the opposite side of the original platform quadrant after the platform had been removed for the positio-

Table 1. Primer sequences.

Gene	Sequence
miR-126-3p mimic	Forward: 5'-UCGUACCGUGAGUAAUAAUGCG-3' Reverse: 5'-CAUUAUUACUCACGGUACGAUU-3'
mimic negative control	Forward: 5'-UUCUCCGAACGUGUCACGUTT-3' Reverse: 5'-ACGUGACACGUUCGGAGAATT-3'
miR-126-3p inhibitor	5'-CGCAUUAUUACUCACGGUACGA-3'
inhibitor negative control	5'-CAGUACUUUUGUGUAGUACAA-3'
miR-126-3p	Forward: 5′- GCATCGTCGTACCGTGAGTAAT -3′ Reverse: 5′- GTGCAGGGTCCGAGGTATTC -3′
U6	Forward: 5′- CTCGCTTCGGCAGCACA -3′ Reverse: 5′- AACGCTTCACGAATTTGCGT -3′
PIK3R2	Forward: 5′- GGCCCTTGGATGGACCTTCT -3′ Reverse: 5′-GCTCAATGGCTTCTATCAGCTTCAC -3′
GAPDH	Forward: 5′- TGACTTCAACAGCGACACCCA -3′ Reverse: 5′- CACCCTGTTGCTGTAGCCAAA -3′

nal navigation experiment training, and the times that the rats traversed the platform within 90 seconds were noted.

Nissl and Hematoxylin-eosin (HE) Staining

Thirty-four days post HI (after Morris Water Maze), the rats were sacrificed. Brain tissue was fixed with formaldehyde and then sliced. Then treated with dimethylbenzene and a gradient of alcohol (absolute, 95%, 80%, and 70%) as usual. Next, the slices were stained with Nissl (C0117; Beyotime, Shanghai, China) or HE (G1120, Solarbio, Beijing, China) solution at 60°C for 50 min. The sections were washed with water first, then dehydrated with alcohol (70%, 80%, and 95%) for two minutes then dimethylbene for five minutes. Under a light microscope, the results were seen and captured in pictures (CX31; Olympus, Tokyo, Japan).

TUNEL Assay

Thirty-four days post-HI, the apoptosis of neurons in the cortex region of the left brain or neurons was quantitated using a cell apoptosis detection kit (C1098, Beyotime, Shanghai, China). Brownish-yellow or brownish-yellow particles with morphological characteristics of apoptotic cells are signs of cell apoptosis. The images were obtained by the light microscope. Apoptotic index = (apoptosis cells / total cells) × 100%.

Immunohistochemistry

Thirty-four days post HI, the silences of cortex tissues of the left brain were administrated with dewaxing, and rehydration as usual. Then, they were removed using boiled citric acid buffer (BCA) for 8 minutes after being incubated with a 3% H_2O_2 methanol solution for 20 minutes. The silences were blocked with 5% bovine serum albumin (BSA) for 18 minutes at room temperature before being incubated with PIK3R2 (1:300; orb76194; Biorbyt, China) antibody for 12 hours at 4°C. Afterward, the sections were rewarmed and incubated with a secondary antibody for 60 min. After visualization using DAB, the tissue specimens were counterstained, dehydrated, cleared, and fixed. Observe the slices under the microscope and count them.

Primary Cortical Neurons Culture

The cortical tissues of Sprague-Dawley rats aged 1 day were collected for separation and elution. The single cell suspension (2-5 × 10^5 /mL) was prepared using fresh complete culture medium and seeded on the poly-L-lysine and laminin-coated cover glasses. The cells were cultured at 37°C with 5% CO_2. The cells were then grown in a medium designed specifically for neurons (Gibco, Rockville, MD, USA), with medium changes occurring every three days.

Oxygen and Glucose Deprivation (OGD) Cell Model

Following the previously described (18), the hypoxic/reoxygenated injury model of cortical neurons was constructed. Cells were cultured in hypoxia for 18 h (5% CO_2, 95% N_2), and reoxygenation for 6 h (5% CO_2).

Cells Groups

Cell groups were included normal control (control), HI, HI+miR-126-3p overexpression (miR-126-3p), HI+PIK3R2 silencing (si-PIK3R2), HI+PIK3R2 silencing negative control (Si-PIK3R2 NC), HI+PIK3R2 overexpression (miR+PIK3R2), HI+PIK3R2 overexpression negative control (miR+ PIK3R2 NC), HI+miR-126-3p overexpression+PIK3R2 overexpression (miR+PIK3R2).

Cortical neuron cells were separately transfected with 100 pmol miR-126-3p mimic (19), 50 nM PIK3R2 siRNA (20), 50 nM PIK3R2 mimic or their equal negative control for 24 h, before HI.

CCK-8 Assay

A 96-well plate with 2% B27-containing media was infected with a cell suspension and cultivated for 3 days at 37°C and 5% CO_2. Twenty-four hours after HI. For 4 hours, 10 L of the CCK-8 solution was added to each well. With the use of a microplate reader, the absorbance was determined at 450 nm.

Acridine Orange (AO) Staining

The cells were collected and cleaned with AO stain buffer (1×). Subsequently, they were resuspended with AO stain buffer (1×) at 1×10^5 cells/well and incubated overnight. Thereafter, cells were stained with AO stain for 15 min without light and washed with PBS. The results were observed and pictured by a fluorescence microscope and analyzed using ImagePro Plus. In this study, we split the picture into red and green channels and analyzed the average gray mean of red fluorescence, which also represents the average fluorescence intensity.

Statistical Analysis

The data was analyzed using Statistic Package for Social Science (SPSS) version 19.0 (IBM Corporation, Armonk, NY, USA). The results were shown as the mean and standard deviation. Data analysis methods employed included one-way analysis of variance and Tukey's test. Differences with $P<0.05$ were considered statistically significant.

Results

High expression of miR-126-3p improved neuronal injury in the cortex

In Figure 1A, the expression of the miR-126-3p group was significantly higher than that of the miR-126-3p NC group, and the level of the inhibitor group was also significantly lower than that of the inhibitor NC group (P<0.05). As demonstrated in Figure 1B, the results of the positioning navigation experiment and spinal exploration experiment of rats in the miR-126-3p group are obviously better than those in other groups (P<0.01). In Figure 1C, the number of Nissl bodies was clearly decreased and the structure of neurons was destroyed in HR neonatal rats compared with normal rats. In addition, the structure and numbers of Nissl bodies were notably improved in the miR-126-3p group versus the HI group (Figure 1D, E). Silence of miR-126-3p aggravated neuron injury paralleled with the HI group.

High levels of miR-126-3p suppressed autophagy and apoptosis in the cortex

The apoptosis rate of the cerebral cortex was increased in the HI group (Figure 2A), decreased in the miR-126-3p group, and significantly increased in the inhibitor group (P<0.01). The levels of LC3II/I, Beclin-1, Bax and Cleved-Caspase-3 increased in the HI group, while the levels of P62 and Bcl-2 decreased, while the protein expression
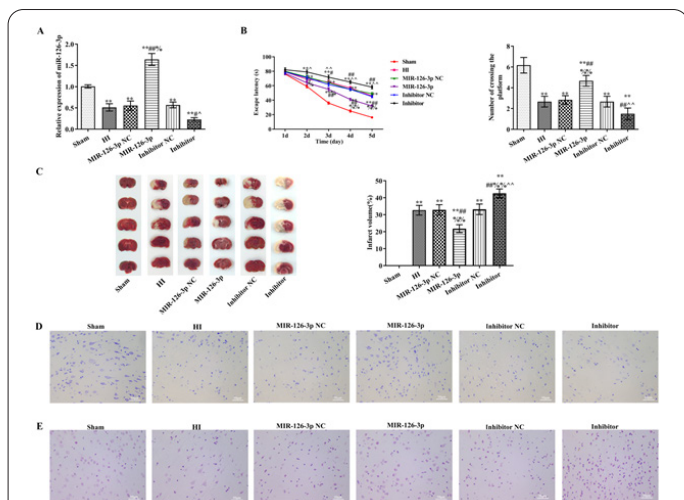

Figure 1. High expression of miR-126-3p protected brain injury. (A) The expression of miR-126-3p in the cortex was analyzed by reverse transcription-polymerase chain reaction (RT-PCR); (B) The escape latency and number of crossing the platform were determined using the Morris water maze test; (C) TTC staining and infarct volumes; (D) Pathology of damaged cortex was observed by HE stating, scale bar = 50 µm; (E) Changes of Nissl bodies in damaged cortex were analyzed by Nissl staining, scale bar = 50 µm. *P<0.05, **P<0.01, compared with sham group; #P<0.05, ##P<0.01, compared with HI group; %P<0.05, %%P<0.01, compared with MIR-126-3p NC group; ^P<0.05, ^^P<0.01, compared with Inhibitor NC group.
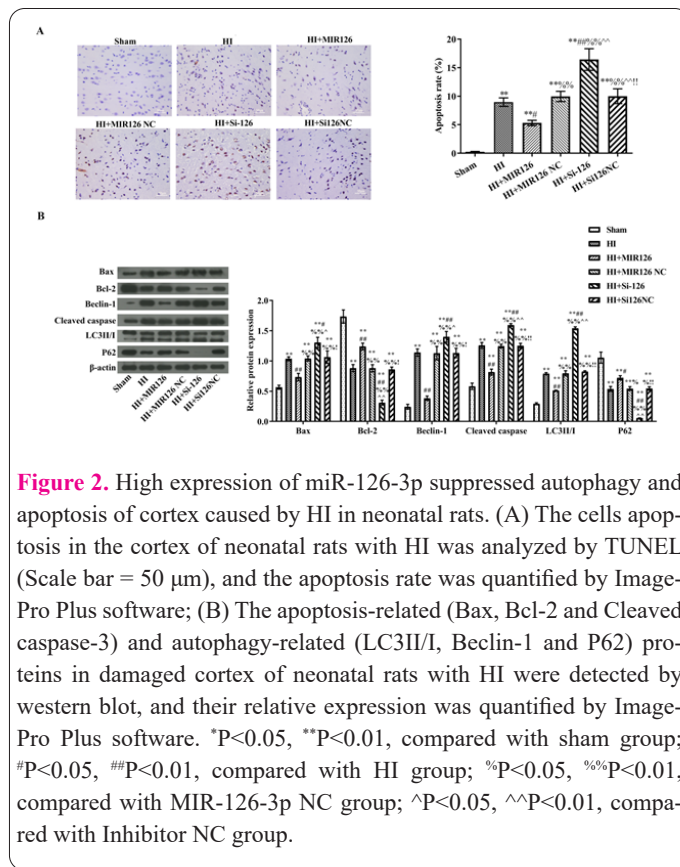

Figure 2. High expression of miR-126-3p suppressed autophagy and apoptosis of cortex caused by HI in neonatal rats. (A) The cells apoptosis in the cortex of neonatal rats with HI was analyzed by TUNEL (Scale bar = 50 µm), and the apoptosis rate was quantified by Image-Pro Plus software; (B) The apoptosis-related (Bax, Bcl-2 and Cleaved caspase-3) and autophagy-related (LC3II/I, Beclin-1 and P62) proteins in damaged cortex of neonatal rats with HI were detected by western blot, and their relative expression was quantified by Image-Pro Plus software. *P<0.05, **P<0.01, compared with sham group; #P<0.05, ##P<0.01, compared with HI group; %P<0.05, %%P<0.01, compared with MIR-126-3p NC group; ^P<0.05, ^^P<0.01, compared with Inhibitor NC group.

level in the miR-126-3p group was completely opposite (Figure 2B), suggesting that miR-126-3p participated in HI-induced autophagy and apoptosis in the cerebral cortex of neonatal rats.

miR-126-3p overexpression inhibited the autophagy and death brought on by OGD

As shown in Figure 3A, the cell viability clearly declined after OGD, and miR-126-3p mimic transfection obviously increased the cell viability (P<0.01). The miR-126-3p expression in each group was confirmed (Figure 3B). The autophagy was increased after injury, but miR-126-3p overexpression inhibited the autophagy of cells through increasing P62 expression, decreasing red fluorescence, LC3II/I and Beclin-1 expression (Figure 3C). Meantime, the apoptosis of cortical neurons (Figure 3D), and Bax, Bcl-2, and cleaved-caspase-3 (Figure 3E) proteins were measured. Similar to this, miR-126-3p overexpression prevented cell death by upregulating Bcl-2 and downregulating Bax and cleaved-caspase-3 expression. However, miR-126-3p silencing increased the severity of autophagy and apoptosis in cells.

PIK3R2 was confirmed as the target gene of miR-126-3p

Treatment with the miR-126-3p mimic reduced the luciferase activity of PIK3R2 containing the wild-type 3'UTR sequence, whereas it did not reduce that of PIK3R2 containing the mutant 3'UTR sequence (Figure 4). This indicates that miR-126-3p can inhibit the transcription or translation of the target gene PIK3R2 by binding to the binding site on PIK3R2-3'UTR, and negatively regulate the expression of PIK3R2 protein. PIK3R2 may be the direct target gene downstream of miR-126-3p.
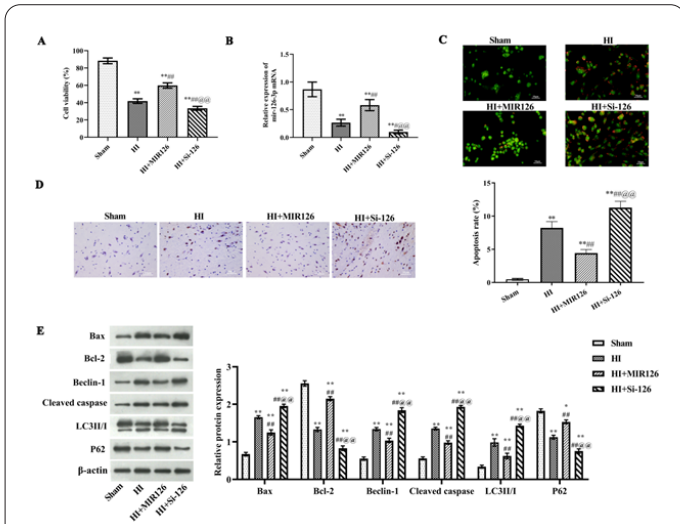
Figure 3. High expression of miR-126-3p suppressed autophagy and apoptosis caused by HI in cortical neurons. (A) The cell viability was analyzed by CCK-8; (B) The expression of miR-126-3p was measured by RT-PCR; (C) The autophagy of cells was observed through AO staining, scale = 50 μm; (D) The apoptosis of cells was analyzed by TUNEL (Scale = 50 μm) and quantified by ImagePro Plus software; (E) The apoptosis-related (Bax, Bcl-2 and Cleaved caspase-3) and autophagy-related (LC3II/I, Beclin-1 and P62) proteins in damaged cortex of neonatal rats with HI were detected by western blot, and their relative expression was quantified by ImagePro Plus software. $^*P<0.05$, $^{**}P<0.01$, compared with sham group; $^#P<0.05$, $^{##}P<0.01$, compared with HI group; $^@P<0.05$, $^{@@}P<0.01$, compared with HI+miR-126 group.

Effects of miR-126-3p on PIK3R2 expression in the damaged cortex caused by HI in neonatal rats and cortical neurons with OGD

The expression of PIK3R2 in the damaged cortex of each group was separately observed through immunohistochemistry (Figure 5A) and western blot (Figure 5B). The PIK3R2 levels in the cortical neurons of each group were analyzed by western blot (Figure 5C). The expression of PIK3R2 was clearly decreased by high miR-126-3p expression, whereas PIK3R2 was strengthened by low miR-126-3p expression.

Effects of miR-126-3p on autophagy by targeting PIK3R2 in cortical neurons with OGD

The roles of silence of PIK3R2 were similar with miR-126-3p overexpression (Figure 6A and B) that autophagy of cells was suppressed through increasing P62 expression, decreasing red fluorescence, LC3II/I and Beclin-1 expression (Figure 6C and D). High expression of PIK3R2 weakened the effects of miR-126-3p overexpression.

Effects of miR-126-3p on apoptosis-related proteins by targeting PIK3R2 in cortical neurons with OGD

When compared to the HI group, miR-126-3p or si-PIK3R2 transfection resulted in higher levels of Bcl-2 and lower levels of Bax and cleaved-caspase-3 (P<0.01) (Figure 7). Furthermore, in contrast to the miR-126-3p group, the Bax and cleaved-caspase-3 protein in the miR+PIK3R2 group was markedly increased, whereas that of the Bcl-2 protein was markedly reduced (P<0.01). It revealed that miR-126-3p suppressed apoptosis of cortical neuron cells with OGD by targeting PIK3R2.

Discussion

The target gene regulated by miRNA accounts for at least 20% of the total genome, which involves the biological process of growth and development of various cells, and then regulates the pathophysiological process of many nervous system diseases. In the process of nervous system
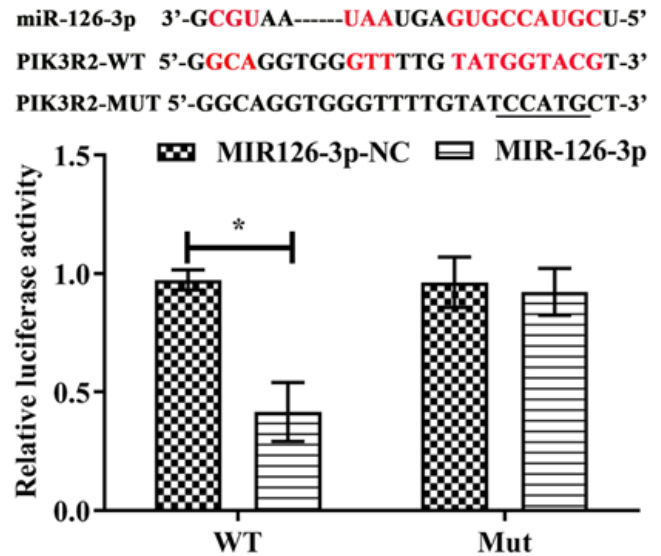

Figure 4. The result of dual luciferase reporter assay. The predicted binding region of miR-126-3p and PIK3R2; Double luciferase report results of the recombinant vector of miR-126-3p and target gene PIK3R2. $^*P<0.05$.
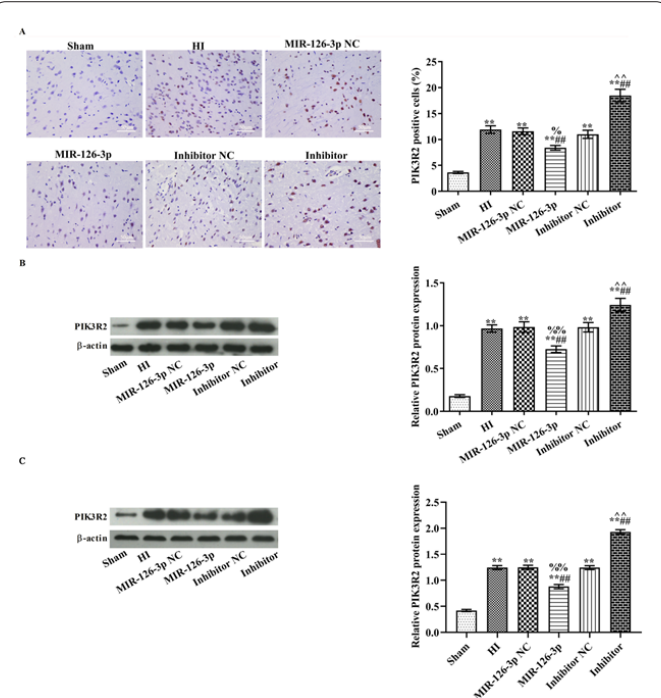

Figure 5. Effects of miR-126-3p on PIK3R2 expression in the damaged cortex of neonatal rats with HI and cortical neurons with OGD. The expression of PIK3R2 in the damaged cortex of neonatal rats with HI was analyzed by immunohistochemistry (scale = 50 μm, A) and western blot (B). The expression of PIK3R2 in the cortical neurons with OGD was analyzed by western blot (C). The expression was quantified by ImagePro Plus software. $^*P<0.05$, $^{**}P<0.01$, compared with sham group; $^#P<0.05$, $^{##}P<0.01$, compared with HI group; $^%P<0.05$, $^{%%}P<0.01$, compared with MIR-126-3p NC group; $^^P<0.05$, $^{^^}P<0.01$, compared with Inhibitor NC group.
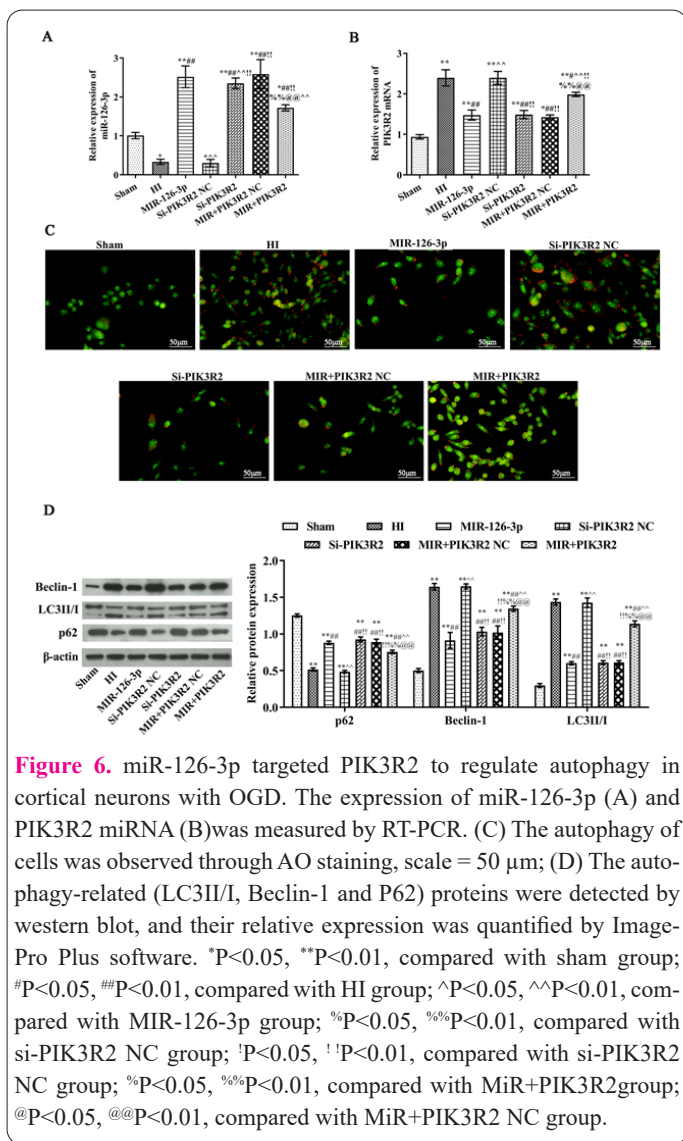
Figure 6. miR-126-3p targeted PIK3R2 to regulate autophagy in cortical neurons with OGD. The expression of miR-126-3p (A) and PIK3R2 miRNA (B)was measured by RT-PCR. (C) The autophagy of cells was observed through AO staining, scale = 50 μm; (D) The autophagy-related (LC3II/I, Beclin-1 and P62) proteins were detected by western blot, and their relative expression was quantified by Image-Pro Plus software. *P<0.05, **P<0.01, compared with sham group; #P<0.05, ##P<0.01, compared with HI group; ^P<0.05, ^^P<0.01, compared with MIR-126-3p group; %P<0.05, %%P<0.01, compared with si-PIK3R2 NC group; ! P<0.05, ! !P<0.01, compared with si-PIK3R2 NC group; ‰P<0.05, ‰‰P<0.01, compared with MiR+PIK3R2group; @P<0.05, @@P<0.01, compared with MiR+PIK3R2 NC group.
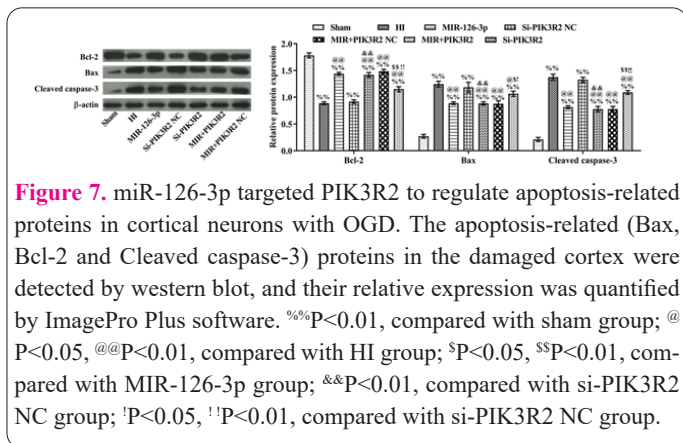

Figure 7. miR-126-3p targeted PIK3R2 to regulate apoptosis-related proteins in cortical neurons with OGD. The apoptosis-related (Bax, Bcl-2 and Cleaved caspase-3) proteins in the damaged cortex were detected by western blot, and their relative expression was quantified by ImagePro Plus software. ‰‰P<0.01, compared with sham group; @P<0.05, @@P<0.01, compared with HI group; $P<0.05, $$P<0.01, compared with MIR-126-3p group; &&P<0.01, compared with si-PIK3R2 NC group; ! P<0.05, ! !P<0.01, compared with si-PIK3R2 NC group.

damage, there is abnormal inactivation or over-expression of miRNA (21-23). MiR-126-3p is specifically expressed in many systems, such as respiratory, digestive, hematopoietic, reproductive and embryonic tissues. The cardiovascular system is where MiR-126-3p exhibits the highest expression specificity (24-26). A study reported that inhibiting PI3K/Akt signaling in the cerebral vascular endothelium, lowering PIK3R2 levels, and reducing blood-brain barrier (BBB) damage after intracerebral hemorrhage are all possible effects of high levels of miRNA-126-3p (19). Wang et al. found that by controlling PIK3R2-mediated inosine phosphate 3-kinase (PI3K)/AKT and nuclear factor kappa B (NF-B), I/R-induced pain hypersensitivity can

be reduced by extracellular vesicles from VSC4.1 neurons repaired by hypoxia that are miR-126-3p-enriched. (17). These reports demonstrated that high levels of miR-126-3p play a protective role in neuronal injury.

Interestingly, Shi et al reported that PIK3R2 is involved in the P13K-AKT pathway, which involves the signal cascade of cell growth, survival, proliferation, movement and morphology, and participates in the cortical stratification of the embryonic brain (27). Reducing or blocking the P13K-AKT pathway will reduce the physiological effect of neuronal apoptosis, thus promoting brain development. Here, we investigated the role of miR-126-3p in the regulation of autophagy and apoptosis in cortical neurons and HI rats. The results showed that miR-126-3p mimic therapy can inhibit PIK3R2 to decrease autophagy and apoptosis in the brain and cortical neurons. Additionally, miR-126-3p overexpression and PIK3R2 silencing reduced the expression of proteins involved in apoptosis. The data obtained from this research were consistent with previous studies (19, 28-30). Additionally, we found that miR-126-3p participated in neuronal autophagy by regulating PIK3R2, and miR-126-3p overexpression inhibited autophagy caused HI in neonatal rats and cortical neurons through down-regulating LC3II/I and Beclin-1, upregulating P62 expression (28,31,32). In clinical practice, drug administration is followed after injury. In our study, we were given the drug administration before the injury, which indicated that miR-126-3p pre-treatment for HI injury was effective. However, the effectiveness of miR-126-3p treatment after HI injury for neonatal rats is not unclear, which needs more experiments to explore its clinical effectiveness.

Autophagy is the adaptive response of cells when nutrition is deficient. Under the stimulation of various factors such as ischemia, cells start an autophagy mechanism to remove damaged mitochondria, prevent apoptosis factors from being released into the cytoplasm, and improve the tolerance of cells to hypoxia, which plays a certain protective role for cells (33-35). Autophagy gene Beclin-1 is involved in the nucleation process of autophagy, and excessive autophagy can significantly up-regulate Beclin-1 expression during the reperfusion period, which will aggravate I/R damage (36,37). In autophagy fluid, LC3 is present as LC3 I and LC3 II. LC3 II joins the creation and growth of the autophagy membrane by adhering to the membrane of the autophagosome. A selective autophagy receptor is created when LC3 II attaches to the p62 protein at the same time as it facilitates the aggregation of ubiquitinated proteins (38-40). p62 protein specifically binds to ubiquitinated proteins, moves them to autophagosomes, and subsequently destroys them in the autophagy pathway along with the ubiquitinated proteins. The activity of selective autophagy is inversely linked with protein levels (41-45). In this study, HI reduced the increase of autophagy through enhancing red fluorescence in AO staining, increased Beclin-1 and LC3II/ I expression in the cortex of neonatal rats and cortical neurons, and decreased P62 expression. After treatment miR-126-3p or silence of PIK3R2 suppressed autophagy caused by HI. This shows that miR-126-3p targeting could be a therapy option for newborns with HI brain injury.

Despite the fact that research on the significance of miR-126-3p is still in its early stages, these discoveries offer a new strategy for the identification and treatment of brain and nervous system disorders. These findings need

to be further investigated to achieve precision medical treatment based on the regulatory mechanism of miR-126-3p and its target genes.

In conclusion, by controlling PIK3R2, miR-126-3p reduced cortical autophagy and apoptosis in HI neonatal rats and cortical neurons, offering a new therapeutic target for brain damage in neonates.

Data Availability Statement
The datasets used and/or analyzed during the present study are available from the corresponding author upon reasonable request.

Conflict of Interests
The authors declare that no conflicts of interest.

Author Contributions
JG: Conceptualization, Methodology, and Software data analysis. JG and XJ: Data curation and Writing of the original draft of the manuscript. XJ and HL: Visualization, Investigation, and Supervision. JG and HL: Writing, Reviewing, and Editing of the manuscript. All authors read and approved the final version of the manuscript.

References

1. Tang Z, Yang F, Dong Y, et al. Midazolam contributes to neuroprotection against hypoxia/reoxygenation-induced brain injury in neonatal rats via regulation of EAAT2. Brain Res Bull 2020; 161: 136-146.

2. Erecinska M, Silver IA. Tissue oxygen tension and brain sensitivity to hypoxia. Respir Physiol 2001; 128(3): 263-276.

3. Solberg R, Longini M, Proietti F, et al. DHA Reduces Oxidative Stress after Perinatal Asphyxia: A Study in Newborn Piglets. Neonatology 2017; 112(1): 1-8.

4. Niu X, Zheng S, Liu H, Li S. Protective effects of taurine against inflammation, apoptosis, and oxidative stress in brain injury. Mol Med Rep 2018; 18(5): 4516-4522.

5. Yang S, Guo L, Wang D, Yang Y, Wang J. Research on Mechanism of miR-106a Nanoparticles Carrying Dexmedetomidine in Regulating Recovery and Metabolism of Nerve Cells in Hypoxia-Reoxygenation Injury. J Biomed Nanotechnol 2022; 18(2): 343-351.

6. Gao Y, Zhang Y, Dong Y, Wu X, Liu H. Dexmedetomidine Mediates Neuroglobin Up-Regulation and Alleviates the Hypoxia/Reoxygenation Injury by Inhibiting Neuronal Apoptosis in Developing Rats. Front Pharmacol 2020; 11: 555532.

7. Jantzie LL, Winer JL, Corbett CJ, Robinson S. Erythropoietin Modulates Cerebral and Serum Degradation Products from Excess Calpain Activation following Prenatal Hypoxia-Ischemia. Dev Neurosci-Basel 2016; 38(1): 15-26.

8. Dingley J, Tooley J, Liu X, et al. Xenon ventilation during therapeutic hypothermia in neonatal encephalopathy: a feasibility study. Pediatrics 2014; 133(5): 809-818.

9. He J, Wang J, Li Y, et al. Effects of umbilical cord mesenchymal stem cells on expression of CYR61, FSH, and AMH in mice with premature ovarian failure. Cell Mol Biol 2021; 67(5): 240-247.

10. Wang X, Hu Y, Fang C, Zhu C. 4cRNA NEAT1 Sponge Adsorption of miR-378 Modulates Activity of Lipopolysaccharide-treated Articular Chondrocytes and Influences the Pathological Development of Osteoarthritis. Altern Ther Health M 2022; 28(6): 103-111.

11. Yang L, Ma T, Zhang Y, Wang H, An R. Construction and Analysis of lncRNA-miRNAmRNA ceRNA Network Identify an Eight-Gene Signature as a Potential Prognostic Factor in Kidney Renal Papillary Cell Carcinoma (KIRP). Altern Ther Health M 2022; 28(6): 42-51.

12. Ouyang YB, Lu Y, Yue S, et al. miR-181 regulates GRP78 and influences outcome from cerebral ischemia in vitro and in vivo. Neurobiol Dis 2012; 45(1): 555-563.

13. Qin Q, Cui L, Zhou Z, Zhang Z, Wang Y, Zhou C. Inhibition of microRNA-141-3p Reduces Hypoxia-Induced Apoptosis in H9c2 Rat Cardiomyocytes by Activating the RP105-Dependent PI3K/AKT Signaling Pathway. Med Sci Monitor 2019; 25: 7016-7025.

14. Sun L, Zhao M, Wang Y, et al. Neuroprotective effects of miR-27a against traumatic brain injury via suppressing FoxO3a-mediated neuronal autophagy. Biochem Bioph Res Co 2017; 482(4): 1141-1147.

15. Qin A, Wen Z, Zhou Y, et al. MicroRNA-126 regulates the induction and function of CD4(+) Foxp3(+) regulatory T cells through PI3K/AKT pathway. J Cell Mol Med 2013; 17(2): 252-264.

16. Gamdzyk M, Doycheva DM, Malaguit J, Enkhjargal B, Tang J, Zhang JH. Role of PPAR-beta/delta/miR-17/TXNIP pathway in neuronal apoptosis after neonatal hypoxic-ischemic injury in rats. Neuropharmacology 2018; 140: 150-161.

17. Wang H, Chen FS, Zhang ZL, Zhou HX, Ma H, Li XQ. MiR-126-3p-Enriched Extracellular Vesicles from Hypoxia-Preconditioned VSC 4.1 Neurons Attenuate Ischaemia-Reperfusion-Induced Pain Hypersensitivity by Regulating the PIK3R2-Mediated Pathway. Mol Neurobiol 2021; 58(2): 821-834.

18. Wei R, Zhang R, Xie Y, Shen L, Chen F. Hydrogen Suppresses Hypoxia/Reoxygenation-Induced Cell Death in Hippocampal Neurons Through Reducing Oxidative Stress. Cell Physiol Biochem 2015; 36(2): 585-598.

19. Xi T, Jin F, Zhu Y, et al. MicroRNA-126-3p attenuates blood-brain barrier disruption, cerebral edema and neuronal injury following intracerebral hemorrhage by regulating PIK3R2 and Akt. Biochem Bioph Res Co 2017; 494(1-2): 144-151.

20. Song L, Li D, Gu Y, et al. MicroRNA-126 Targeting PIK3R2 Inhibits NSCLC A549 Cell Proliferation, Migration, and Invasion by Regulation of PTEN/PI3K/AKT Pathway. Clin Lung Cancer 2016; 17(5): e65-e75.

21. Ben Y, Hao J, Zhang Z, et al. Astragaloside IV Inhibits Mitochondrial-Dependent Apoptosis of the Dorsal Root Ganglion in Diabetic Peripheral Neuropathy Rats Through Modulation of the SIRT1/p53 Signaling Pathway. Diabet Metab Synd Ob 2021; 14: 1647-1661.

22. Liu Y, Ding Z, Zhang J, Song C, Zhang L, Liu Y. Highly Sensitive Detection of miRNA-155 Using Molecular Beacon-Functionalized Monolayer MoS2 Nanosheet Probes with Duplex-Specific Nuclease-Mediated Signal Amplification. J Biomed Nanotechnol 2021; 17(6): 1034-1043.

23. Jeyaseelan K, Lim KY, Armugam A. MicroRNA expression in the blood and brain of rats subjected to transient focal ischemia by middle cerebral artery occlusion. Stroke 2008; 39(3): 959-966.

24. Guenther SP, Schrepfer S. miR-126: a potential new key player in hypoxia and reperfusion? Ann Transl Med 2016; 4(19): 377.

25. Gao S, Gao H, Dai L, et al. miR-126 regulates angiogenesis in myocardial ischemia by targeting HIF-1alpha. Exp Cell Res 2021; 409(2): 112925.

26. Qu Q, Liu L, Cui Y, et al. miR-126-3p containing exosomes derived from human umbilical cord mesenchymal stem cells pro-

mote angiogenesis and attenuate ovarian granulosa cell apoptosis in a preclinical rat model of premature ovarian failure. Stem Cell Res Ther 2022; 13(1): 352.

27. Shi X, Lim Y, Myers AK, et al. PIK3R2/Pik3r2 Activating Mutations Result in Brain Overgrowth and EEG Changes. Ann Neurol 2020; 88(6): 1077-1094.

28. Pan J, Qu M, Li Y, et al. MicroRNA-126-3p/-5p Overexpression Attenuates Blood-Brain Barrier Disruption in a Mouse Model of Middle Cerebral Artery Occlusion. Stroke 2020; 51(2): 619-627.

29. Venkat P, Cui C, Chopp M, et al. MiR-126 Mediates Brain Endothelial Cell Exosome Treatment-Induced Neurorestorative Effects After Stroke in Type 2 Diabetes Mellitus Mice. Stroke 2019; 50(10): 2865-2874.

30. Bassand K, Metzinger L, Naim M, et al. miR-126-3p is essential for CXCL12-induced angiogenesis. J Cell Mol Med 2021; 25(13): 6032-6045.

31. Liu Y, Mo C, Mao X, Lu M, Xu L. Increasing miR-126 Can Prevent Brain Injury after Intracerebral Hemorrhage in Rats by Regulating ZEB1. Contrast Media Mol I 2022; 2022: 2698773.

32. Fei L, Zhang N, Zhang J. Mechanism of miR-126 in hypoxia-reoxygenation-induced cardiomyocyte pyroptosis by regulating HMGB1 and NLRP3 inflammasome. Immunopharm Immunot 2022; 44(4): 500-509.

33. Bouchelaghem R, Mader S, Gaboury L, Messarah M, Boumendjel M, Boumendjel A. Estrogens desensitize MCF-7 breast cancer cells to apelin-induced autophagy and enhanced growth under estrogen starvation: a possible implication in endocrine resistance. Cell Mol Biol 2022; 68(9): 113-124.

34. Rong Y, Fan J, Ji C, et al. USP11 regulates autophagy-dependent ferroptosis after spinal cord ischemia-reperfusion injury by deubiquitinating Beclin 1. Cell Death Differ 2022; 29(6): 1164-1175.

35. Sun P, Nie M. Effect and mechanism of Angelic Shaoyaosan mediated AMPK/SIRT1 positive feedback loop to promote autophagy and regulate the systemic inflammatory response in acute

pancreatitis. Cell Mol Biol 2021; 67(2): 101-108.

36. Tavernarakis N. Regulation and Roles of Autophagy in the Brain. Adv Exp Med Biol 2020; 1195(33.

37. Grishchuk Y, Ginet V, Truttmann AC, Clarke PG, Puyal J. Beclin 1-independent autophagy contributes to apoptosis in cortical neurons. Autophagy 2011; 7(10): 1115-1131.

38. Pattingre S, Tassa A, Qu X, et al. Bcl-2 antiapoptotic proteins inhibit Beclin 1-dependent autophagy. Cell 2005; 122(6): 927-939.

39. Nakamura S, Akayama S, Yoshimori T. Autophagy-independent function of lipidated LC3 essential for TFEB activation during the lysosomal damage responses. Autophagy 2021; 17(2): 581-583.

40. Fan S, Yue L, Wan W, et al. Inhibition of Autophagy by a Small Molecule through Covalent Modification of the LC3 Protein. Angew Chem Int Edit 2021; 60(50): 26105-26114.

41. Azizi Dargahlou, S., Iriti, M., Pouresmaeil, M., Goh, L. P. W. MicroRNAs; their therapeutic and biomarker properties. Cell Mol Biomed Rep 2023; 3(2): 73-88. doi: 10.55705/cmbr.2022.365396.1085

42. Kanwal, N., Al Samarrai, O., Al-Zaidi, H. M. H., Mirzaei, A., Heidari, M. Comprehensive analysis of microRNA (miRNA) in cancer cells. Cell Mol Biomed Rep 2023; 3(2): 89-97. doi: 10.55705/cmbr.2022.364591.1070.

43. Sasani S, Rashidi Monfared S, Mirzaei AR. Identification of some Echinophora platyloba miRNAs using computational methods and the effect of these miRNAs in the expression of TLN2 and ZNF521 genes in different human body organs. Cell Mol Biomed Rep 2024; 4(1): 43-53. doi: 10.55705/cmbr.2023.386145.1100.

44. Liu WJ, Ye L, Huang WF, et al. p62 links the autophagy pathway and the ubiqutin-proteasome system upon ubiquitinated protein degradation. Cell Mol Biol Lett 2016; 21: 29.

45. Deng Z, Lim J, Wang Q, et al. ALS-FTLD-linked mutations of SQSTM1/p62 disrupt selective autophagy and NFE2L2/NRF2 anti-oxidative stress pathway. Autophagy 2020; 16(5): 917-931.